




1-Bit Reconfigurable Metasurfaces for Frequency and Polarization Control in 5G FR2 Band

William O. F. Carvalho , Osvaldo N. Oliveira Jr. , and J. R. Mejía-Salazar 

Abstract— Reconfigurable metasurfaces can be used for manipulating wavefronts, but their scalability using available fabrication methods is limited owing to their complex geometries. This study presents a simplified metasurface with dynamic tunability in frequency and polarization within the 5G frequency range 2 (FR2) band. The meta-cells are made of square-ring resonators with PIN diode connections only in x -axis, which can manipulate wavefronts based on diode 1-bit switch (ON and OFF). Numerical simulations demonstrate high extinction ratios of up to 21.5 dB and cross-talk peaks of 22.3 dB, making this design promising for future 5G applications with 1-bit reconfigurable metasurfaces.

Keywords— 5G, FR2, Frequency Selectivity, Reconfigurable Metasurfaces, Polarization Control.

I. INTRODUCTION

Metasurfaces are man-made surfaces which can be used to manipulate electromagnetic waves through a two-dimensional array of subwavelength structures [1], [2], thus transcending the limitations of natural materials [3]. Despite their advantages such as minimal losses and cost efficiency, metasurfaces are hindered by their passive designs. This limitation becomes evident in scenarios necessitating dynamic wavefront adjustments, a requirement for high-frequency mobile communications in future 5G and 6G networks. These drawbacks are being addressed with the development of mechanisms and technologies for reconfigurable metasurfaces that can be dynamically tuned to control transmission, reflection, absorption, and polarization. With such control, these reconfigurable metasurfaces can be utilized in various applications, including frequency selective surfaces (FSSs)[4], beam steering and beamforming[5], [6], wavefront manipulation [7], [8], spectrum control [9], and sensing [10], [11], [12]. In fact, reconfigurable and programmable metasurfaces may impact wireless communications by allowing for higher data rates, improved coverage, and reduced

latency [13], [14]. In future 6G mobile networks, reconfigurable metasurfaces may enable even more sophisticated wireless communication systems [15], [16], [17].

The reconfigurability of metasurfaces is facilitated by various physical principles, allowing for dynamic stimuli through the use of electric or magnetic fields, thermal, optical, and/or mechanical effects [18]. These mechanisms permit real-time adjustment of electromagnetic responses, rendering metasurfaces highly active and tunable. Among the successful approaches for achieving this goal are the utilization of varactors [19], [20], [21], Schottky [22], [23] or positive-intrinsic-negative (PIN) diodes [24], [25]. These components have been employed to deflect, split, or modulate the incident wave according to specific requirements [26]. PIN diodes, in particular, serve as dynamic binary switching elements that alter the electromagnetic response of metasurfaces based on applied bias voltages [27]. With low insertion losses, they maintain high efficiency in metasurface designs, facilitating compact integration with the meta-cells. By dynamically changing the bias voltages applied to the PIN diodes, digital-coding metasurfaces can encode complex electromagnetic functionalities [28]. Digital-coding metasurfaces can perform wave manipulation using n -bit coding for each metasurface cell [1], with PIN diodes typically utilized for 1-bit coding (ON and OFF states). These elements can be altered independently, creating heterogeneous phase profiles and changing transmitted/reflected beam deflections [28], [29], [30].

The approaches above to tailor electromagnetic responses are still limited in terms of scalability owing to the requirement of conductive vias for bias circuits, additional microstrips for feeding active elements, complex geometries, and sophisticated fabrication techniques. In this work, we present a reconfigurable metasurface that utilizes PIN diodes for dynamic control of frequency and polarization selectivity. The concept involves conductive square-ring resonator-based (SRR) metamaterials operating in the 5G frequency range 2 (FR2), centered at $f = 26$ GHz. Our approach combines the conventional frequency selective surfaces (FSSs) with in-line PIN diodes performing strategic switching of the surface currents and capacitive effects between parallel conductors, thereby changing the resonant frequency through only 1-bit switching. The PIN diodes, which can be switched between ON/OFF states, enable the metasurface to function as a transmitting, reflecting, or polarization filtering device, according to the incidence of linearly polarized (LP) electric field ($\mathbf{E} \parallel \hat{\mathbf{x}}$, $\mathbf{E} \parallel \hat{\mathbf{y}}$) or circularly polarized (CP) fields. The device exploits conventional materials used in radiofrequency (RF) and could be easily fabricated with well-established techniques. Numerical results indicate

William O. F. Carvalho, Sao Carlos Institute of Physics, University of Sao Paulo, CP 369, 13560-970, São Carlos, SP, Brasil, e-mail: williamofcarvalho@gmail.com; Osvaldo N. Oliveira Jr., Sao Carlos Institute of Physics, University of Sao Paulo, CP 369, 13560-970, São Carlos, SP, Brasil, e-mail: chu@ifsc.usp.br; J. R. Mejía-Salazar, National Institute of Telecommunications (Inatel), 37540-000, Santa Rita do Sapucaí, Brazil, e-mail: jrmejia@inatel.br. This work has been partially funded by the project XGM-AFCCT-2024-3-1-1 supported by xGMobile-EMBRAPII-Inatel Competence Center on 5G and 6G Networks, with financial resources from the PPI IoT/Manufatura 4.0 from MCTI grant number 052/2023, signed with EMBRAPII. We also acknowledge financial support from the Brazilian agency National Council for Scientific and Technological Development-CNPq (314671/2021-8), FAPESP (2023/08999-9, 2018/22214-6), FAPEMIG (APQ-04523-23, PPE-00124-23), and RNP, with resources from MCTIC, Grant No.01245.020548/2021-07, under the Brazil 6G project of the Radiocommunication Reference Center (Centro de Referência em Radiocomunicações - CRR) of the National Institute of Telecommunications (Instituto Nacional de Telecomunicações - Inatel), Brazil.

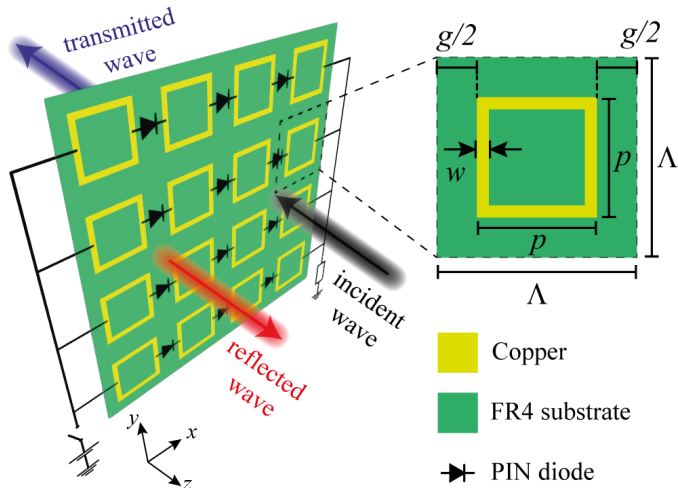


Fig. 1: Schematic of reconfigurable metasurface by PIN diodes. The inset shows the material composition and geometrical parameters of the unit meta-cell.

Extinction Ratios (ERs) up to $ER = 21.5$ dB at $f = 26$ GHz for PIN diodes considered in ON and OFF states, whilst cross-talk (CT) peaks as high as $|CT_{x,y}|$ (dB) = 22.3 dB were obtained.

II. METHODOLOGY

A schematic representation of the proposed metasurface is shown in Fig. 1, which comprises a two-dimensional periodic arrangement of metallic meta-cells equally distributed along the xy -plane with period Λ . The meta-cells are made of copper SRR with length p , width w and thickness t_{Cu} , grown on a t_s thick FR4 substrate. The gap between the adjacent resonators is $g = \Lambda - p$. On the horizontal gaps (x -axis) are considered PIN diodes in series connected in the middle of the vertical ring strip for the electric tunability. It is worth noticing that horizontal PIN diodes are polarized all at once through the single key for ON and OFF states. A black arrow is used to illustrate an incident electromagnetic wave, whilst the red and blue arrows are for reflected and transmitted waves, respectively. We first optimized the unit meta-cells parameters to exhibit frequency selectivity at 5G FR2 band, centered at $f = 26$ GHz. The full-wave simulations were carried out using the finite element method (FEM) using the commercial software COMSOL Multiphysics. For a realistic simulations, we considered the materials values taken from experimental reports for RF, with the copper conductivity $\sigma_{Cu} = 5.998 \times 10^7$ S/m and the low-loss FR4 permittivity of $\epsilon_{FR} = 4.4$ and loss tangent $\tan \delta = 0.019$ [31]. The respective thicknesses were $t_{Cu} = 35$ μ m and $t_s = 1.6$ mm. The optimization of the geometric parameters of the unit meta-cell led to $\Lambda = 4.6$ mm, $p = 2.3$ mm, $w = 0.24$ mm and $g = 2.3$ mm. This latter gap allows a feasible distance to weld the PIN diodes, which were considered as perfect electric conductors (PEC) contact ($\sigma_d^{ON} = \infty$ S/m) for ON state and perfect insulator contact ($\sigma_d^{OFF} = 0$ S/m) for OFF state. The simulations consider only one unit meta-cell through Floquet periodic boundary conditions along x and y boundaries. In z boundary were set a transmitter and receiver ports to

launch and receive the wave to the metasurface, respectively, for calculating transmission/reflection coefficient. Through the retrieval method, one can use the S -parameters to feature the metasurface and calculate the meta-cell effective permittivity and permeability, given by [32]

$$\epsilon_{\text{eff}} = \frac{c}{j\pi t_s f} \frac{1 - S_{21} - S_{11}}{1 + S_{21} + S_{11}}, \quad (1)$$

$$\mu_{\text{eff}} = \frac{c}{j\pi t_s f} \frac{1 - S_{21} + S_{11}}{1 + S_{21} - S_{11}}, \quad (2)$$

where c is the speed of light in vacuum and f is the working frequency. S_{21} and S_{11} are the scattering parameters for transmission and reflection, respectively. This allows the analysis of the metasurface performance as a function of PIN diodes states. Results were obtained within the range of $16 \text{ GHz} < f < 36 \text{ GHz}$, namely, centered in FR2 frequencies, for normal incidence.

III. RESULTS AND DISCUSSION

The transmittances for LP waves under normal incidence are shown in Fig. 2(a). The black and red lines represent the x -polarization ($\mathbf{E} \parallel \hat{\mathbf{x}}$) and y -polarization ($\mathbf{E} \parallel \hat{\mathbf{y}}$) respectively, featuring the resonant response features of the metasurface. Solid lines correspond to resonance responses with inactive PIN diodes (OFF state), while dotted lines signify activated PIN diodes (ON state). A prominent resonance at $f = 26$ GHz is observed for $\mathbf{E} \parallel \hat{\mathbf{x}}$, well within the 5G FR2 band, indicating significant reflection. However, for $\mathbf{E} \parallel \hat{\mathbf{y}}$, there is a slight displacement in resonance centered at $f = 28.5$ GHz. This deviation is primarily due to the insertion of in-line PIN diodes, causing a breaking of symmetry despite the entirely symmetrical geometry of the SRR meta-cells. The influence of PIN diodes, depicted solely along the x -axis in Fig. 1, is particularly notable on electromagnetic field coupling and resonance conditions in this direction. Introducing in-line PIN diodes along the y -axis, or removing those along the x -axis, would restore symmetry to the structure. Consequently, both LP resonances would overlap.

When the PIN diodes are activated (ON state), they serve as closed contacts between horizontally adjacent meta-cells. This action results in a significant alteration of the capacitance between these parallel conductors. Hence, at $f = 26$ GHz, $\mathbf{E} \parallel \hat{\mathbf{x}}$ does not exhibit wave coupling at the metasurface, evident from the black-dotted line in Fig. 2(a). The transmittance shows a flat response across the 5G FR2 band (around S_{21} (dB) = -4.5 dB), indicating a high ER between ON and OFF states, calculated as $ER_{\mathbf{E} \parallel \hat{\mathbf{x}}}^{\text{ON,OFF}} = 21.5$ dB. Furthermore, although $\mathbf{E} \parallel \hat{\mathbf{y}}$ within the FR2 band does not exhibit a flat response regardless of the PIN diode states, this polarization can still be considered transmitted within the same range. In the ON state, $\mathbf{E} \parallel \hat{\mathbf{y}}$ only experiences a slight resonance shift from $f = 28.5$ GHz to $f = 30.5$ GHz. This shift is associated with the conductive behavior of the PIN diodes, contributing to the capacitance effects in the horizontal strip conductors. These results indicate that our design is suitable for reconfiguration in both frequency and polarization selectivity applications using a single 1-bit switching. To evaluate polarization selectivity performance,

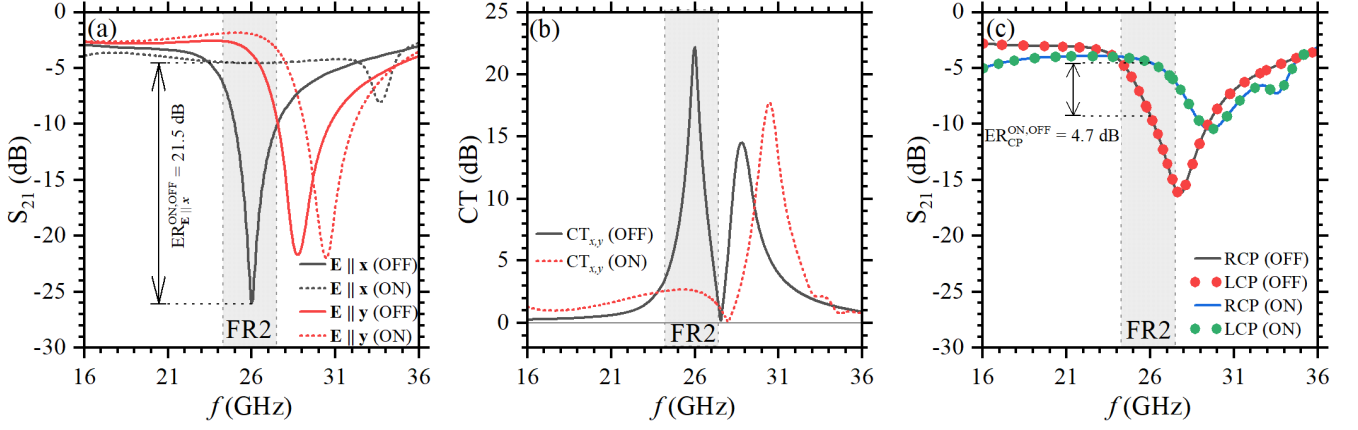


Fig. 2: Reconfigurable transmittances S_{21} (dB) as a function of frequency in the range around 5G FR2 band. (a) LP as $\mathbf{E} \parallel \hat{\mathbf{x}}$ (black) and $\mathbf{E} \parallel \hat{\mathbf{y}}$ (red) responses for PIN diodes as OFF (solid lines) and ON (dotted) states. (b) CT between the $\mathbf{E} \parallel \hat{\mathbf{x}}$ and $\mathbf{E} \parallel \hat{\mathbf{y}}$ polarizations for OFF (black-solid line) and ON (red-dotted line) states. (c) RCP and LCP transmittance responses for PIN diodes as OFF and ON states.

we employ the CT parameter, which quantifies the disparities between x - and y -polarization

$$|\text{CT}_{x,y} \text{ (dB)}| = |S_{21}^x \text{ (dB)} - S_{21}^y \text{ (dB)}|, \quad (3)$$

given in dB. The superindexes x and y indicate the transmission coefficient S_{21} for $\mathbf{E} \parallel \hat{\mathbf{x}}$ and $\mathbf{E} \parallel \hat{\mathbf{y}}$, respectively. Fig. 2(b) shows high CT peaks for PIN diodes as OFF (black-solid line) and ON (red-dotted line) states. Polarization filtering can also be manipulated by the horizontal PIN diodes within the 5G FR2 band. The high CT peak of $|\text{CT}_{x,y} \text{ (dB)}| = 22.3$ dB is found at $f = 26$ GHz in OFF state and $|\text{CT}_{x,y} \text{ (dB)}| = 19.6$ dB is found at $f = 30.5$ GHz in ON state, evidencing the potential for polarization tunable filtering. In Fig. 2(c) we extend the analysis for CP wavefronts, i.e., $\mathbf{E} = E_x \hat{\mathbf{x}} \pm i E_y \hat{\mathbf{y}}$, where the sign \pm denotes the right-handed CP (RCP) or left-handed CP (LCP). As expected, the RCP and LCP transmittances overlap each other in both ON and OFF states. Herein, frequency selection is observed only at $f = 26$ GHz with $\text{ER}_{\text{CP}}^{\text{ON,OFF}} = 4.7$ dB. The resonance dip in $f = 27.8$ GHz for OFF state (black-solid line and red-dotted line) is caused by contributions of the $\mathbf{E} \parallel \hat{\mathbf{x}}$ and $\mathbf{E} \parallel \hat{\mathbf{y}}$ components seen in Fig. 2(a). A similar combination

is seen for the ON state (blue-solid line and green-dotted line), where the flat response for $\mathbf{E} \parallel \hat{\mathbf{x}}$ is combined with a slight blue-shift of $\mathbf{E} \parallel \hat{\mathbf{y}}$.

The reconfigurability of the metasurface is closely tied to the varied responses of the effective permittivity (ϵ_{eff}) and permeability (μ_{eff}) depending on the polarization state of the PIN diodes. Fig. 3 illustrates the ϵ_{eff} (black lines) and μ_{eff} (red lines) in both OFF (solid) and ON (dotted) states for all analyzed polarizations, using Eq.(1) and Eq.(2). A significant change in ϵ_{eff} occurs for $\mathbf{E} \parallel \hat{\mathbf{x}}$ (refer to Fig. 3(a)). The inset highlights the suppression of the permittivity peak when the PIN diode is in the ON state, a factor that strongly influences the metasurface response. Conversely, the effective parameters for $\mathbf{E} \parallel \hat{\mathbf{y}}$ (Fig. 3(b)) and CP (Fig. 3(c)) show subtle changes, resulting in the small resonance displacement in Fig. 2(b).

Fig. 4 shows the normalized electric fields $|\mathbf{E}|$ at $f = 26$ GHz. The states of the PIN diodes, ON and OFF, affect the resonant coupling at the SRR. Specifically, for $\mathbf{E} \parallel \hat{\mathbf{x}}$, the coupled field (Fig. 4(a)) decreases when the PIN diode is activated (Fig. 4(b)). This modulation can be explained by

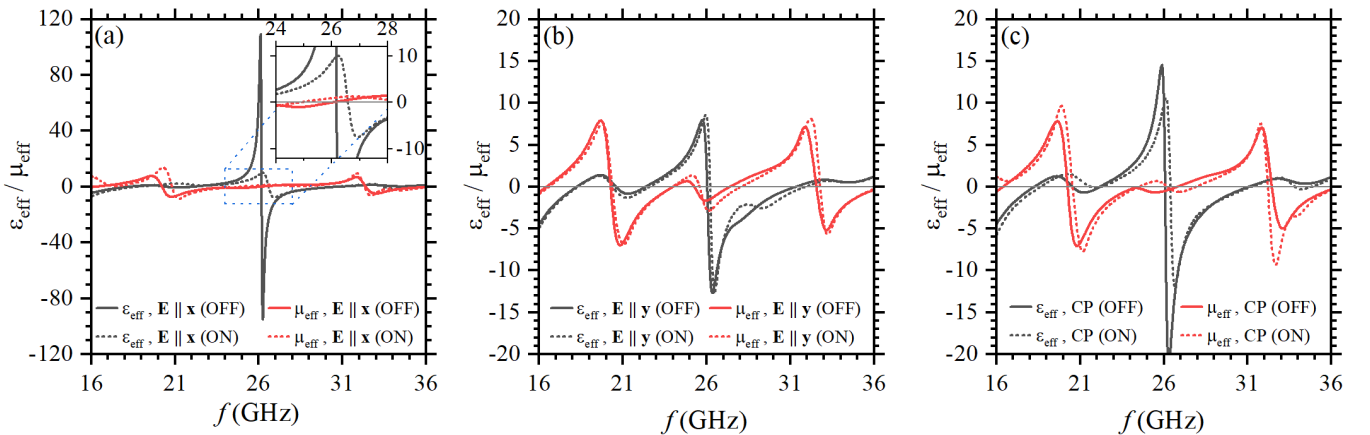


Fig. 3: The effective permittivities ϵ_{eff} (black) and permeabilities μ_{eff} (red) for (a) $\mathbf{E} \parallel \hat{\mathbf{x}}$, (b) $\mathbf{E} \parallel \hat{\mathbf{y}}$ and (c) circular polarization states, considering PIN diodes in OFF (solid lines) and ON states (dotted lines).

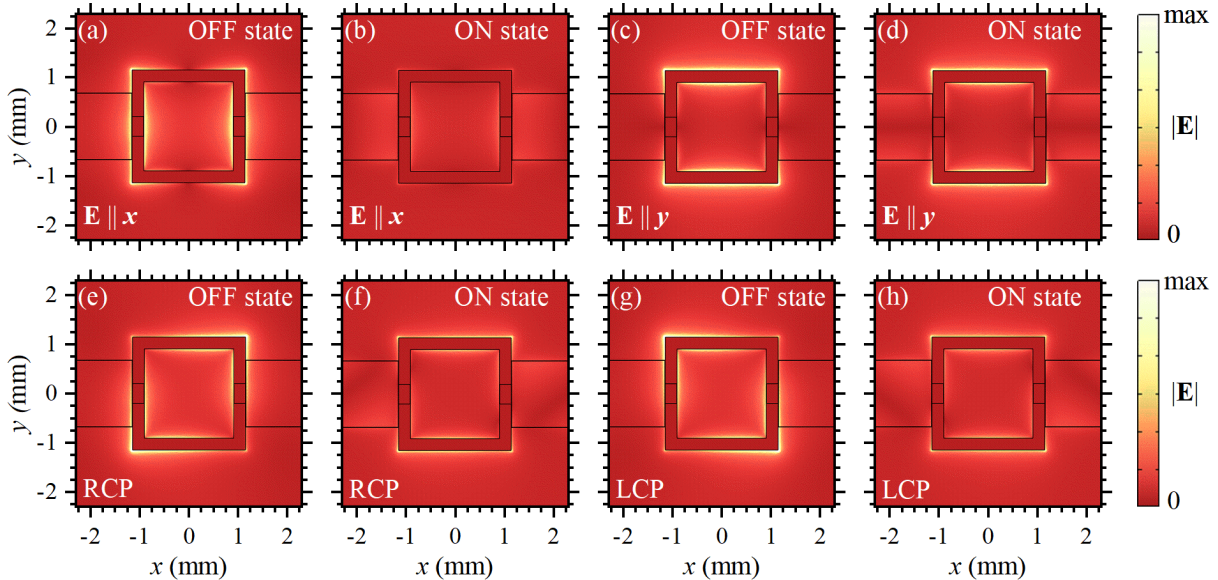


Fig. 4: Normalized electric field $|\mathbf{E}|$ at $f = 26$ GHz for (a)-(b) $\mathbf{E} \parallel \hat{x}$, (c)-(d) $\mathbf{E} \parallel \hat{y}$, (e)-(f) RCP and (g)-(h) LCP for PIN diodes in x -axis as in OFF and ON states.

considering the parallel plate capacitor model for vertical parallel conductor strips and the dielectric separator. The introduction of a conductive link between the strips, by polarizing the PIN diode, induces capacitance modulation that shifts the resonance conditions and changes ε_{eff} , as depicted in Fig. 3(a). Conversely, in the corresponding OFF (Fig. 4(c)) and ON (Fig. 4(d)) states, there is no significant coupling modulation observed for \mathbf{E} parallel to \hat{y} , highlighting the metasurface's role as both frequency and polarization selective. Examining CP wavefronts, rotational symmetries are evident in Figs. 4(e)-(h), indicating the metasurface's functionality for this more complex polarization state. In the OFF states (illustrated in Figs. 4(e) and (g)), resonance features display a differential phase of $\pm\pi/2$, as evidenced by the $\pi/2$ -rotational symmetry of the near-field profile along the z -axis. In Figs. 4(f) and (h), the ON state cases highlight a symmetry for rotations of π around the $y = 0$ -axis. This symmetry arises from the capacitance modulation by PIN diodes along the parallel conductor strips. Therefore, our proposal works well for both LP and CP states of the incident wavefronts in 5G wireless communications within the FR2 band.

IV. CONCLUSIONS

We have shown that metasurfaces can be reconfigurable to modulate meta-cell properties dynamically, for applications in frequency and polarization selectivity. By strategically placing PIN diodes exclusively along the x -axis to connect adjacent SRR meta-cells, the metasurface exhibited the ability to alter transmission, reflection, and polarization signals through 1-bit switching—i.e., toggling the PIN diodes between OFF and ON states. This control mechanism relies on capacitance modulation between the vertical conductive strips, contingent upon the state of the PIN diodes, as evidenced by changes in effective parameters. Moreover, our findings revealed a notable enhancement in ER, with $\text{ER}_{\mathbf{E} \parallel \hat{x}}^{\text{ON,OFF}} = 21.5$ dB, signifying

strong frequency selectivity. Additionally, we observed a peak CT of $|\text{CT}_{x,y} \text{ (dB)}| = 22.3$ dB within the 5G FR2 frequency range. This proposal offers a framework for establishing a responsive mechanism to regulate transmission, reception, and polarization across a wide spectrum, pertinent to high-frequency mobile communication networks.

REFERENCES

- [1] Q. Cheng, L. Zhang, J. Y. Dai, W. Tang, J. C. Ke, S. Liu, J. C. Liang, S. Jin, and T. J. Cui, "Reconfigurable intelligent surfaces: Simplified-architecture transmitters—from theory to implementations," *Proceedings of the IEEE*, vol. 110, no. 9, pp. 1266–1289, 2022.
- [2] O. A. M. Abdelraouf, Z. Wang, H. Liu, Z. Dong, Q. Wang, M. Ye, X. R. Wang, Q. J. Wang, and H. Liu, "Recent advances in tunable metasurfaces: materials, design, and applications," *ACS Nano*, vol. 16, no. 9, pp. 13 339–13 369, 2022.
- [3] V. G. Ataloglou, S. Taravati, and G. V. Eleftheriades, "Metasurfaces: physics and applications in wireless communications," *Natl. Sci. Rev.*, vol. 10, no. 8, p. nwad164, 2023.
- [4] E. M. Materon, H. R. D. Figueiras, E. C. Vilas Boas, F. R. Gómez, F. R. P. Cavalcanti, Y. C. B. Silva, A. Cerqueira S, F. A. P. de Figueiredo, L. L. Mendes, O. N. Oliveira, and J. R. Mejía-Salazar, "Flexible metasurfaces as sub-6 GHz frequency selective surfaces for 5G applications," *Journal of Applied Physics*, vol. 134, no. 14, 2023.
- [5] V. G. Ataloglou, G. Egorov, J. Kim, G. Xu, A. H. Dorrah, A. Ohadi, M. Kim, and G. V. Eleftheriades, "Static and reconfigurable huygens' metasurfaces: Use in antenna beamforming and beam steering," *IEEE Antennas Propag. Mag.*, vol. 64, no. 4, pp. 73–84, 2022.
- [6] N. Ashraf, T. Saeed, H. Taghvaei, S. Abadal, V. Vassiliou, C. Liaskos, A. Pitsillides, and M. Lestas, "Intelligent beam steering for wireless communication using programmable metasurfaces," *IEEE Trans. Intell. Transp. Syst.*, 2023.
- [7] J. He, T. Dong, B. Chi, and Y. Zhang, "Metasurfaces for terahertz wavefront modulation: a review," *J. Infrared Millim. Terahertz Waves*, vol. 41, no. 6, pp. 607–631, 2020.
- [8] Y. Wang, S. Li, H. Wang, L. Feng, B. Tan, Y. Tan, R. Su, J. Wu, C. Zhang, B. Jin *et al.*, "Broadband and efficient asymmetric wavefront manipulation via terahertz polarization-selective metasurface," *Appl. Phys. Lett.*, vol. 121, no. 15, 2022.
- [9] J. Y. Dai, J. Zhao, Q. Cheng, and T. J. Cui, "Independent control of harmonic amplitudes and phases via a time-domain digital coding metasurface," *Light Sci. Appl.*, vol. 7, no. 1, p. 90, 2018.

- [10] G. Lan, M. F. Imani, P. Del Hougne, W. Hu, D. R. Smith, and M. Gorlatova, "Wireless sensing using dynamic metasurface antennas: Challenges and opportunities," *IEEE Commun. Mag.*, vol. 58, no. 6, pp. 66–71, 2020.
- [11] M. Beruete and I. Jáuregui-López, "Terahertz sensing based on metasurfaces," *Adv. Opt. Mater.*, vol. 8, no. 3, p. 1900721, 2020.
- [12] W. O. F. Carvalho, O. N. Oliveira, and J. R. Mejía-Salazar, "Magnetochiroptical nanocavities in hyperbolic metamaterials enable sensing down to the few-molecule level," *J. Chem. Phys.*, vol. 160, no. 7, 2024.
- [13] T. Sharma, A. Chehri, and P. Fortier, "Reconfigurable intelligent surfaces for 5G and beyond wireless communications: A comprehensive survey," *Energies*, vol. 14, no. 24, p. 8219, 2021.
- [14] H. Taghvaei, A. Jain, S. Abadal, G. Gradoni, E. Alarcón, and A. Cabellos-Aparicio, "On the enabling of multi-receiver communications with reconfigurable intelligent surfaces," *IEEE Trans. Nanotechnol.*, vol. 21, pp. 413–423, 2022.
- [15] I. F. Akyildiz, A. Kak, and S. Nie, "6G and beyond: The future of wireless communications systems," *IEEE Access*, vol. 8, pp. 133 995–134 030, 2020.
- [16] M. Khalily, O. Yurduseven, T. J. Cui, Y. Hao, and G. V. Eleftheriades, "Engineered electromagnetic metasurfaces in wireless communications: Applications, research frontiers and future directions," *IEEE Commun. Mag.*, vol. 60, no. 10, pp. 88–94, 2022.
- [17] G. C. Alexandropoulos, N. Shlezinger, I. Alamzadeh, M. F. Imani, H. Zhang, and Y. C. Eldar, "Hybrid reconfigurable intelligent metasurfaces: Enabling simultaneous tunable reflections and sensing for 6G wireless communications," *IEEE Veh. Technol. Mag.*, 2023.
- [18] C. Liu, F. Yang, S. Xu, and M. Li, "Reconfigurable metasurface: A systematic categorization and recent advances," *Electromagn. Sci.*, vol. 1, no. 4, pp. 1–23, 2023.
- [19] Z. Wu and A. Grbic, "Serrodyne frequency translation using time-modulated metasurfaces," *IEEE Trans. Antennas Propag.*, vol. 68, no. 3, pp. 1599–1606, 2019.
- [20] R. Phon, M. Lee, C. Lor, and S. Lim, "Multifunctional reflective metasurface to independently and simultaneously control amplitude and phase with frequency tunability," *Adv. Opt. Mater.*, vol. 11, no. 14, p. 2202943, 2023.
- [21] X. Yang, E. Wen, D. Bharadia, and D. F. Sievenpiper, "Multifunctional metasurface: Simultaneous beam steering, polarization conversion and phase offset," *IEEE Trans. Antennas Propag.*, 2024.
- [22] E. Vassos, J. Churm, J. Powell, C. Viegas, B. Alderman, and A. Feresidis, "Air-bridged schottky diodes for dynamically tunable millimeter-wave metamaterial phase shifters," *Sci. Rep.*, vol. 11, no. 1, p. 5988, 2021.
- [23] X. Liu, H. Chen, S. Liang, M. Zhang, Z. Jiang, S. Fan, and Y. Sun, "Ultrabroadband electrically controllable terahertz modulation based on gaas schottky diode structure," *APL Photonics*, vol. 6, no. 11, 2021.
- [24] Y. Fan, T. Qiao, F. Zhang, Q. Fu, J. Dong, B. Kong, and H. Li, "An electromagnetic modulator based on electrically controllable metamaterial analogue to electromagnetically induced transparency," *Sci. Rep.*, vol. 7, no. 1, p. 40441, 2017.
- [25] Z. Wu, J. Zhao, K. Chen, and Y. Feng, "An active metamaterial absorber with ultrawideband continuous tunability," *IEEE Access*, vol. 10, pp. 25 290–25 295, 2022.
- [26] C. Cui, J. Ma, K. Chen, X. Wang, T. Sun, Q. Wang, X. Zhang, and Y. Zhang, "Active and programmable metasurfaces with semiconductor materials and devices," *Crystals*, vol. 13, no. 2, p. 279, 2023.
- [27] C. Huang, C. Zhang, J. Yang, B. Sun, B. Zhao, and X. Luo, "Reconfigurable metasurface for multifunctional control of electromagnetic waves," *Adv. Opt. Mater.*, vol. 5, no. 22, p. 1700485, 2017.
- [28] Q. Ma, Q. Xiao, Q. R. Hong, X. Gao, V. Galdi, and T. J. Cui, "Digital coding metasurfaces: From theory to applications," *IEEE Antennas Propag. Mag.*, vol. 64, no. 4, pp. 96–109, 2022.
- [29] C. Fu, L. Han, C. Liu, X. Lu, and Z. Sun, "Reflection-type 1-bit coding metasurface for radar cross section reduction combined diffusion and reflection," *J. Phys. D: Appl. Phys.*, vol. 53, no. 44, p. 445107, 2020.
- [30] W. Liu, J. Y. Dai, Y. M. Zhang, M. K. Sun, L. Zhang, Y. Li, H. J. He, T. J. Cui, and Q. Cheng, "Wideband polarization-insensitive 1-bit phase manipulations with co- and cross-polarized conversions for LP and CP waves," *Laser Photonics Rev.*, p. 2400049, 2024.
- [31] S. Shamoony, W. Y. Zhou, F. Shahzad, W. Ali, and H. Subbyal, "Integrated sub-6 GHz and millimeter wave band antenna array modules for 5G smartphone applications," *AEU - Int. J. Electron. Commun.*, vol. 161, p. 154542, 2023.
- [32] A. A. MUSAED, S. S. Al-Bawri, W. M. Abdulkawi, K. Aljaloud, Z. Yusoff, and M. T. Islam, "High isolation 16-port massive MIMO antenna based negative index metamaterial for 5G mm-wave applications," *Sci. Rep.*, vol. 14, no. 1, p. 290, 2024.